

This is a repository copy of *A study of the influence of plasma–molecule interactions on particle balance during detachment*.

White Rose Research Online URL for this paper:

<https://eprints.whiterose.ac.uk/id/eprint/171844/>

Version: Published Version

---

**Article:**

(2021) A study of the influence of plasma–molecule interactions on particle balance during detachment. Nuclear Materials and Energy. 100922. ISSN: 2352-1791

<https://doi.org/10.1016/j.nme.2021.100922>

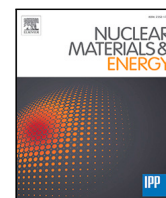
---

**Reuse**

This article is distributed under the terms of the Creative Commons Attribution-NonCommercial-NoDerivs (CC BY-NC-ND) licence. This licence only allows you to download this work and share it with others as long as you credit the authors, but you can't change the article in any way or use it commercially. More information and the full terms of the licence here: <https://creativecommons.org/licenses/>

**Takedown**

If you consider content in White Rose Research Online to be in breach of UK law, please notify us by emailing [eprints@whiterose.ac.uk](mailto:eprints@whiterose.ac.uk) including the URL of the record and the reason for the withdrawal request.



# A study of the influence of plasma–molecule interactions on particle balance during detachment

Kevin Verhaegh<sup>a,b,c,\*</sup>, Bruce Lipschultz<sup>b</sup>, James Harrison<sup>a</sup>, Basil Duval<sup>c</sup>, Chris Bowman<sup>b</sup>, Alexandre Fil<sup>b,a</sup>, Daljeet Singh Gahle<sup>d,a</sup>, David Moulton<sup>a</sup>, Omkar Myatra<sup>b,a</sup>, Artur Perek<sup>e</sup>, Christian Theiler<sup>c</sup>, Mirko Wensing<sup>c</sup>, MST1 team<sup>1</sup>, TCV team<sup>2</sup>

<sup>a</sup> Culham Centre for Fusion Energy, Culham, United Kingdom

<sup>b</sup> York Plasma Institute, University of York, United Kingdom

<sup>c</sup> Swiss Plasma Centre, École Polytechnique Fédérale de Lausanne, Lausanne, Switzerland

<sup>d</sup> SUPA, University of Strathclyde, Glasgow, United Kingdom

<sup>e</sup> DIFFER, Eindhoven, The Netherlands

## ARTICLE INFO

### Keywords:

Tokamak divertor

Molecules

Plasma

Plasma spectroscopy

Particle balance

Detachment

## ABSTRACT

In this work we provide experimental insights into the impact of plasma–molecule interactions on the target ion flux decrease during divertor detachment achieved through a core density ramp in the TCV tokamak. Our improved analysis of the hydrogen Balmer series shows that plasma–molecule processes are strongly contributing to the Balmer series intensities and substantially alter the divertor detachment particle balance.

We find that Molecular Activated Recombination (MAR) ion sinks from  $H_2^+$  (and possibly  $H^-$ ) are a factor  $\sim 5$  larger than Electron–Ion Recombination (EIR) and are a significant contributor to the observed reduction in the outer divertor ion target flux. Molecular Activated Ionisation (MAI) appears to be substantial during the detachment onset, but further research is required into its magnitude given its uncertainty.

Plasma–molecule interactions enhance the Balmer line series emission strongly near the target as detachment proceeds. This indicates enhancements of the Lyman series, potentially affecting power balance in the divertor. As those enhancements vary spatially in the divertor and are different for different transitions, they are expected to result in a separation of the  $Ly\beta$  and  $Ly\alpha$  emission regions. This may have implications for the treatment and diagnosis of divertor opacity.

The demonstrated enhancement of the Balmer series through plasma–molecule processes potentially poses a challenge to using the Balmer series for understanding and diagnosing detachment based only on atom–plasma processes.

## 1. Introduction

Divertor detachment is expected to be a crucial aspect for handling the power exhaust of future fusion devices, such as ITER and DEMO [2]. During detachment, a range of atomic and molecular processes result in simultaneous power, particle and momentum losses from the plasma to neutral species or to photons (e.g. radiative power loss). This results in a simultaneous reduction of the target plasma temperature ( $T_t$ ) and the ion target flux  $\Gamma_t$ . Such changes in the plasma facilitate large reductions in the target heat flux ( $q_t$ ) as shown in Eq. (1) where  $\gamma$  is the sheath transmission coefficient and  $\epsilon$  is the surface recombination energy that

is deposited when an  $H^{+3}$  ion converts to an atom (13.6 eV) and afterwards to a molecule (+2.2 eV) [3].

$$q_t = \Gamma_t(\gamma T_t + \epsilon) \quad (1)$$

This simultaneous reduction of the ion target flux ( $\Gamma_t$ ) and the target temperature requires target pressure ( $p_t$ ) loss according to the sheath-target conditions (Eq. (2)). That target pressure loss can be facilitated through volumetric momentum losses [4–9] and may involve an upstream pressure loss as indicated in previous research on TCV [10].

\* Corresponding author at: Culham Centre for Fusion Energy, Culham, United Kingdom.

E-mail address: [kevin.verhaegh@ukaea.uk](mailto:kevin.verhaegh@ukaea.uk) (K. Verhaegh).

<sup>1</sup> See author list of “B. Labit et al. 2019 Nucl. Fusion 59 086020”.

<sup>2</sup> See author list of “S. Coda et al. 2019 Nucl. Fusion 59 112023”.

<sup>3</sup> In this work we use H for hydrogen as the available reaction rates/emission coefficients are only available for hydrogen. The discharge discussed in this work is, however, a deuterium discharge. The impact of such assumptions are further discussed in Section 2 following [1].

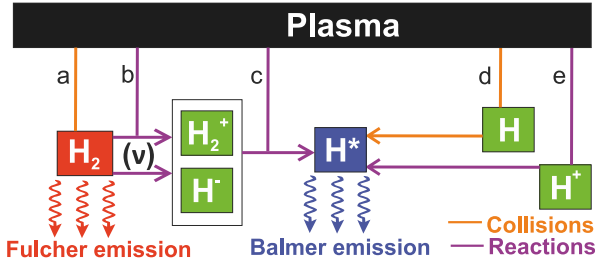


**Fig. 1.** Schematic overview of important plasma-molecule and plasma-atom collisions (in orange) and reactions (in magenta) discussed in this work. (a) Collisions between the plasma and  $H_2$  excite the molecule rovibronically; (b) Reactions between the plasma and  $H_2(v)$  result in the formation of  $H_2^+$  and  $H^-$ ; (c) Reactions between the plasma and  $H_2^+$  (and possibly  $H^-$ ), which can result in excited neutral atoms ( $H^*$ ) and Balmer line emission; (d) Collisions between electrons and  $H$  excite  $H^*$ , resulting in Balmer line emission; (e) Electron-ion recombination reactions with  $H^+$  resulting in excited  $H^*$  and Balmer line emission.

$$\Gamma_i \propto p_i / T_i^{1/2} \quad (2)$$

A reduction of the ion flux requires either a reduction of the ion source or an increase in the ion sink according to particle balance (Eq. (3)). Here,  $\Gamma_i$  ( $\Gamma_r$ ) is the divertor ion source (sink) and  $\Gamma_u$  is a net ion flow from upstream towards (positive)/away from (negative) the target.  $\Gamma_i$  is generally thought to be much larger than  $\Gamma_u$ :  $\Gamma_i \ll \Gamma_u \rightarrow \Gamma_i \approx \Gamma_i - \Gamma_r$ ; high recycling conditions [9–13] and Fig. 2.

$$\Gamma_i = \Gamma_i - \Gamma_r + \Gamma_u \quad (3)$$

The divertor ion source ( $\Gamma_i$ ) is strongly connected to power balance as each ionisation event requires a certain amount of energy ( $E_{ion}$ ) [9–13]. The ionisation source ( $\Gamma_i$ ) becomes limited by the power flux flowing into the recycling/ionisation region ( $q_{rec}$ ) if the power flux loss due to ionisation ( $\Gamma_i E_{ion}$ ) becomes comparable (within a factor of two [10]) to  $q_{rec}$ . Impurity radiation is often (one of) the main power dissipation processes reducing the power crossing the SOL ( $q_{SOL}$ ) before the power enters the recycling region ( $q_{rec}$ ). Particle, power and momentum balance are thus all connected through Eqs. (1)–(3) (where  $q_i = q_{rec} - E_{ion}\Gamma_i$ ). All three balances play an important role in detachment [8,10,14]. Most studies of detachment have focused on the target ion current in detachment and how plasma-atom interactions affect power, momentum and particle balance, leading  $\Gamma_i$  to drop.

Modifications in those three balances are driven by plasma-atom [10,11,15] and plasma-molecule interactions. To investigate the impact of plasma-molecule interactions further, we must distinguish between two different ‘types’ of plasma-molecule interactions: *collisions* between the plasma and  $H_2$  and *reactions* from the plasma chemistry of  $H_2$ . A schematic overview of such *reactions* and *collisions* are shown in Fig. 1. Collisions between the plasma and  $H_2$  lead to rovibronic excitation [16–22] (Fig. 1a).

Reactions between the plasma and  $H_2$  leads to  $H_2$  dissociation and to the formation of  $H_2^+$  and  $H^-$  [16,17,23] as illustrated in 1b. Reactions which result in the *formation* (for  $T_e < 4$  eV) of  $H_2^+$  and  $H^-$  can be greatly enhanced by the population of higher vibrationally excited states ( $v$ ) which are populated through plasma-molecule *collisions* [16] (Fig. 1a).  $H_2^+$  and  $H^-$  react with the plasma (Fig. 1c), *breaking down*  $H_2^+$  and  $H^-$ , resulting in excited (\*) neutrals which emit atomic hydrogen line emission [1,18,23,24] - see Fig. 1c. The cross-sections for the reactions which form  $H_2^+$  and  $H^-$  can have strong isotope dependencies which are still being debated in literature [25,26]. In particular the dissociative attachment ( $H_2 + e^- \rightarrow H^- + H$ ) cross-section is thought to be strongly diminished for deuterium ( $^2_1H^+$ ) and more so for tritium ( $^3_1H^+$ ) compared to protium ( $^1_1H^+$ ) [26].

Most experimental investigations into the impact of molecules on plasma-edge physics in tokamaks have utilised  $H_2$  Fulcher band (590–640 nm) emission measurements [16,19] which arise from electronic excitation of  $H_2$  due to plasma-molecule *collisions* (step a in Fig. 1). Those measurements directly show that the plasma is interacting with the molecules resulting in rovibronic (meaning electronically – resulting in Fulcher band emission, vibrationally –  $H_2(v)$  and rotationally) excitation [16,17,19]. That information, combined with model or simulation results, has been used in studies to infer information on *reactions* between the plasma and molecules [16,19].

Although it was suspected from DIII-D and JET studies [19,27] that the  $H\alpha$  emission in the divertor may be enhanced by plasma-molecule interactions, the impact of excited atoms from plasma-molecule interactions on the atomic spectra has not yet been studied quantitatively in tokamak divertors.

### 1.1. The effect of plasma-molecule interactions on particle, energy and momentum balance

There are multiple chains of plasma-molecule reactions involving  $H_2$ ,  $H_2^+$  and  $H^-$  that ‘effectively’ ionise neutrals and recombine ions; a summary can be found in [1]. One example is molecular charge exchange ( $H_2 + H^+ \rightarrow H_2^+ + H$ ) resulting in the formation of  $H_2^+$  which dissociatively recombines with an electron:  $H_2^+ + e^- \rightarrow H + H$ . When comparing the inputs and outputs of those reactions, we observe that an ion was effectively recombined: Molecular Activated Recombination – MAR. Alternatively at higher temperatures, molecular reactions can activate the ionisation of a plasma neutral – Molecular Activated Ionisation – MAI.

Both plasma-molecule collisions and reactions impact the plasma power balance. Collisions between the plasma and the molecules transfer kinetic energy from the plasma to the molecular cloud [28–30]. Although emission (and thus radiation) from molecular ( $H_2$ ) bands occurs, the radiative losses from such processes are experimentally estimated to be insignificant — in agreement with EDGE2D-Eirene modelling [20]. Radiative energy loss also occurs from excited atoms formed after plasma-molecule reactions [1,23,24] (step c in Fig. 1).

Plasma-molecule collisions transfer momentum from the plasma to the molecules, effectively acting as a momentum sink [14,28–31]. Apart from collisions, the molecular charge exchange reaction ( $H_2 + H^+ \rightarrow H_2^+ + H$ ) also results in momentum losses [29,31].

### 1.2. The scope of this paper

In this work we employ a new technique [1] to experimental Balmer spectra from the TCV tokamak to extract information about plasma-molecule interactions. Our results indicate plasma-molecule interactions strongly increase hydrogenic line emission and modify particle balance significantly during detachment. MAI starts to contribute to the ion target flux at around the detachment onset. For the TCV case studied, MAR is  $\sim 5$  times larger than the EIR ion sink (atomic processes). The final result is that the inclusion of plasma sources and sinks due to plasma-molecule processes significantly alters the picture of particle balance derived from plasma-atom processes alone.

The Balmer line emission enhancement during detachment attributed to plasma-molecule interactions: (1) is strongest near the target while the  $H_2$  Fulcher emission region tracks the ionisation region; suggesting that different plasma-molecule interactions occur at different locations of the TCV divertor; (2) are indicative of increases of the Lyman series, which could potentially affect power balance in the divertor; (3) could have implications for divertor opacity effects as it can result in a spatial separation between the  $L\gamma\alpha$  and  $L\gamma\beta$  emission regions.

## 2. Spectral analysis techniques of inferring information on plasma–molecule interaction from the Balmer spectra

We have used the analysis technique ‘Balmer Spectroscopy of Plasma-Molecular Interactions’ - ‘BaSPMI’ [1] to investigate the spectroscopic data in this work. For simplicity we define Balmer line emission from electron-impact excitation of H and EIR of  $H^+$  as “atomic” contributions to the Balmer line emission while we define Balmer line emission arising from excited atoms after plasma interactions with  $H_2$ ,  $H_2^+$  and  $H^-$  as contributions to the Balmer line emission arising from “plasma–molecule interactions”. The total atomic line emission is then the sum of the “atomic” ( $H$ ,  $H^+$ ) and “plasma–molecule interaction” ( $H_2$ ,  $H_2^+$ ,  $H^-$ ) contributions [1]. BaSPMI uses chordal-integrated brightness measurements of  $H\alpha$ ,  $H\beta$ , as well as two other medium-n Balmer lines (e.g.  $n = 5-7$ ) together with Stark inferred electron densities; and uses data from ADAS [32,33], YACORA (On the Web) [23,24] as well as AMJUEL [34].

The goal of BaSPMI is “to quantify the contribution of plasma–molecule interactions to the Balmer lines and use this to provide quantitative estimates of the influence of molecules on power losses, particle (ion) sources/sinks and Balmer line emission” [1]. This builds upon previous atomic analysis technique developed by the authors in [35] and works on the principle that certain plasma–molecule reactions result in excited atoms emitting atomic line emission, which is more dominant for lower-n Balmer lines ( $H\alpha$ ,  $H\beta$ ) than higher-n ones.

The profile of the various emission contributions vary continuously along the line of sight. However, the analysis technique (see [1]) simplifies the emission profiles as a ‘dual slab’ model (with a hot and cold temperature) along the line of sight. That approach has been verified using SOLPS-ITER simulations for both TCV (density scan) and MAST-U (density and  $N_2$  puffing scan) using ‘synthetic testing’. Although there is a strong spatial separation of the various emission and reaction regions in those simulations, the analysis of the chordal-integrated brightnesses still provides similar estimates of the chordal-integrated atomic and molecular ion sources/sinks as is obtained when summing those sources/sinks from the simulation directly along the line of sight. The ‘synthetic testing’, employed in [1], uses data tables from [25] for the  $H_2 + H^+ \rightarrow H_2^+ + H$  rate (for deuterium) and default AMJUEL data tables (protium) for other rates related to  $H_2^+$  and  $H^-$  to post-process the SOLPS-ITER simulations to obtain the  $H_2^+$  and  $H^-$  densities. Similar agreement between the analysis result and the result directly obtained from the simulation is obtained when either the AMJUEL base rate (protium) or the ‘remapped ( $T_e/2$ )’ AMJUEL rate (Eirene default for deuterium at the time) for  $H_2^+ + H^+ \rightarrow H_2^+ + H$  are used. Furthermore, the emission contributions from  $H_2^+$  and  $H^-$  have been turned off individually in the synthetic testing in to verify that the analysis correctly identifies their presence [1].

Although the cross-sections for forming  $H_2^+$  and  $H^-$  have strong isotope dependencies (see Section 1), BaSPMI does not use these rates [1] and instead detects the excited neutrals arising from reactions breaking down  $H_2^+$  and  $H^-$ . However, BaSPMI does rely on population coefficients from Yacora (on the Web) [23,24] and MAR/MAI rates from AMJUEL [36], which are available for just protium. Nevertheless, the analysed discharge is a deuterium discharge. We provide the analysis in this work with this caveat and increased availability of data for deuterium would benefit this analysis [1].

Although the cross-section for dissociative attachment are thought to be strongly reduced for deuterium discharges [26], we keep the hydrogenic line emission arising from plasma interactions with  $H^-$  as a free parameter in this work. Removing that degree of freedom does not change any of the presented results beyond their uncertainty margins as the emission attributed to  $H^-$  will now be attributed to  $H_2^+$  instead and the MAR/ $H\alpha$  photon ratio for  $H^-$  and  $H_2^+$  are similar within experimental uncertainties [1]. We have bundled the contributions of  $H_2^+$  and  $H^-$  together in terms of their Balmer line emission and MAR/MAI ion sinks/sources throughout this work as distinguishing between those two is beyond the scope of this paper.

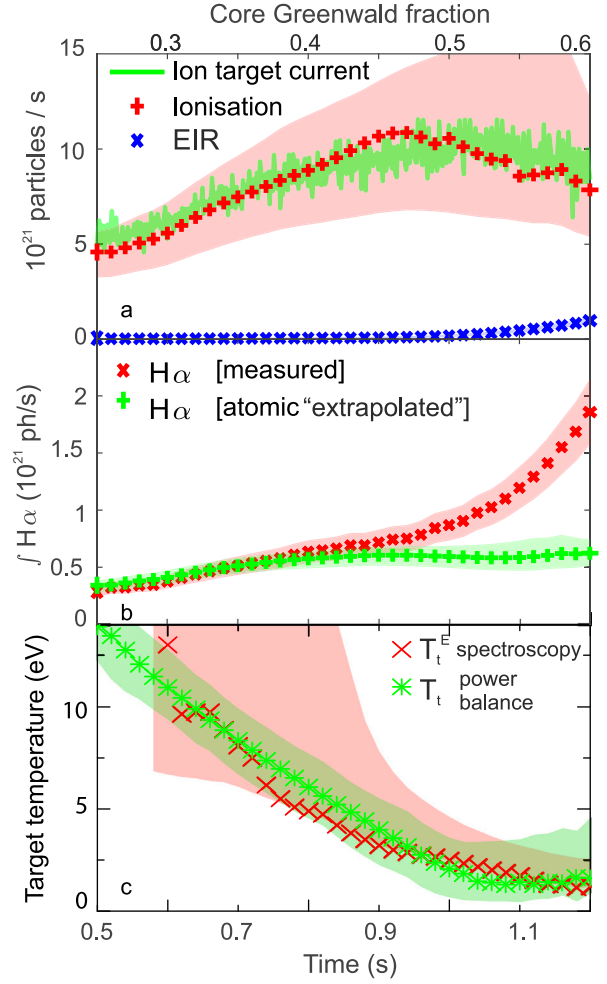


Fig. 2. Inferred particle balance only considering plasma–atom interactions. (a) Particle balance (ion target current) shown together with estimated atomic ion source, electron–ion recombination (EIR) sink. (b) Measured total  $H\alpha$  in the divertor together with the estimated atomic part of the  $H\alpha$  emission. (c) Target temperature estimates (based on the spectroscopically inferred excitation temperature -  $T_e^E$  and a temperature estimate obtained from power balance.

Source: Adopted from [10].

## 3. Experimental results on TCV

The TCV discharge used for this study (#56567) has previously been analysed in detail from the point of view of atomic interactions only [10]. As shown in Fig. 2d, #56567 has a single null divertor shape with spectroscopy lines of sight intersecting the outer divertor leg along most of its length. #56567 is an L-mode Deuterium plasma with  $I_p = 340$  kA discharge in reversed field (i.e. ion grad-B drift away from the primary x-point) without additional impurity seeding (although intrinsic carbon impurities are present and are an important power loss process [10]). This discharge has been repeated multiple times with different spectroscopy settings to obtain sufficient spectroscopic coverage for BaSPMI as well as to obtain Fulcher band measurements. The reproducibility of these discharges is adequate for this [10].

First we investigate particle balance of this discharge 2 based on a spectroscopic analysis [35] which assigns all medium-n Balmer line emission to atomic interactions only. Under TCV attached conditions we observe a linear increase of the ion target current (Fig. 2a). Such a linear increase is predicted by analytical models, due partially to the reduction of upstream temperature during the ramp of the upstream density [10]. The total ion target current,  $I_i$ , stops rising linearly at



around a Greenwald fraction of 0.33 (detachment onset) and rolls over around a Greenwald fraction of 0.4. We observe that the atomic electron-ion recombination sink only becomes relevant at latest phase of the discharge (where the target temperature  $T_t \sim 1$  eV - Fig. 2c), while the ionisation rate drops before this phase at the detachment onset (where  $T_t \sim 4$  eV - Fig. 2c). Our atomic analysis has shown that the reduction of the ionisation source occurs as the power entering the recycling region becomes 'limited' to sustain sufficient ionisation - 'power limitation' [10], which has been theorised [11,37] and suspected from experiments previously [11,15].

A bifurcation starts to occur between the measured and estimated "atomic extrapolated"  $H\alpha$  emission at the detachment onset ( $T_t \sim 4$  eV - Fig. 2c), Fig. 2b, and become increasingly more significant ( $T_t < 2$  eV - Fig. 2c) as the divertor becomes colder. This is indicative of an additional source of  $n = 3$  excited atoms. The 'atomic'  $H\alpha$  emission is based on the analysis of the medium- $n$  Balmer lines, assuming the higher- $n$  Balmer lines are only populated by "atomic" interactions [35].

While the expected  $H_2$  densities from SOLPS-ITER simulations under these density/temperature conditions (e.g. detached  $T_t < 5$  eV plasma,  $n_e \sim 10^{20} \text{ m}^{-3}$ ) contribute less than 1% of the measured  $H\alpha$  emission [1], plasma-molecule interactions involving  $H_2^+$  (and possibly  $H^-$ ) could explain the additional  $H\alpha$  brightness after detachment [1]. Such plasma-molecule interactions lead to losses (sinks) for ions in the plasma through Molecular Activated Recombination (MAR). Other possible additional sources of  $n = 3$  excited atoms, such as  $Ly\beta$  opacity and plasma-molecule interactions with hydrocarbons, are estimated to only increase the  $H\alpha$  emission by a few percent for these TCV conditions [1]. Therefore, we assume that the additional  $H\alpha$  emission is due to plasma-molecule interaction.

### 3.1. The evolution of detachment with plasma-molecule interactions

In Fig. 3 we apply the full self-consistent BaSPMI atomic and molecular spectroscopic analysis chain to identify the impact of plasma-molecule interactions on three measured Balmer lines measured during this discharge. Initially only electron impact excitation (of H) emission plays a role for all three Balmer lines (Fig. 3).

As the target temperature drops, first plasma-molecule interactions and later electron-ion recombination form an increasingly larger part of the Balmer line emission (Fig. 3). Near the detachment onset (Core Greenwald fraction  $n_e/n_{GW} \sim 0.43$ ), the region of strong electron impact excitation 'detaches' from the target (see Fig. 3b-d), leaving a region where enhanced Balmer line emission from  $H_2^+$  (and possibly  $H^-$ ) as well as EIR occur. This region expands as the divertor becomes colder, following the movement of the electron-impact excitation region. In the latest phases of the discharge ( $n_e/n_{GW} > 0.5$ ), "plasma-molecule interactions" are the dominant excitation process for  $H\alpha$  and  $H\beta$  near the target. For  $H\gamma$  and  $H\delta$  (not shown), the impact of plasma-molecule interactions is significant, but most of the emission is from EIR. At this phase of the discharge, the fractions of  $H\beta$ ,  $H\gamma$  emission associated with plasma-molecule interactions (but not the actual brightnesses - see Fig. 4) are higher 25 cm above the target than near the target due to a lack of electron-ion recombination ( $T_e \sim [2.5 - 4]$  eV). The fact that plasma-molecule interactions are an important excitation process for  $H\alpha$  and  $H\beta$  emission suggests that such interactions result in significant hydrogenic radiation and thus power balance, which will be investigated in future work.

To provide some insight into the evolution of different kinds of plasma-molecule interactions during detachment, we compare the brightness profile (line-integrated along the divertor leg and therefore also intersecting the private flux and common flux regions) of a part of the  $H_2$  Fulcher band (600-614 nm) with that of the various  $H\alpha$  excitation sources in Fig. 4. Fulcher band emission occurs when electrons have sufficient energy for plasma-molecule collisions to result in electronically excited molecules. A first observation is that the Fulcher emission penetrates throughout the divertor leg in the attached phase.

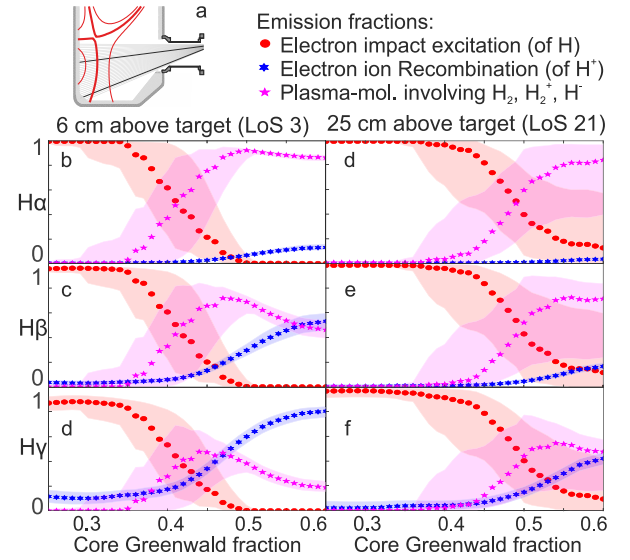


Fig. 3. (a) Magnetic equilibrium of the investigated discharge with spectroscopic line of sight coverage (two chords are highlighted which are used in Fig. 3. b-f) The  $H\alpha$ ,  $H\beta$ ,  $H\gamma$  self-consistent emission fractions as function of core Greenwald fraction for two different chords (Fig. 2) in terms of "atomic" contributions (electron impact excitation (of H) and EIR (of  $H^+$ ) and "plasma-molecule interaction" related contributions.

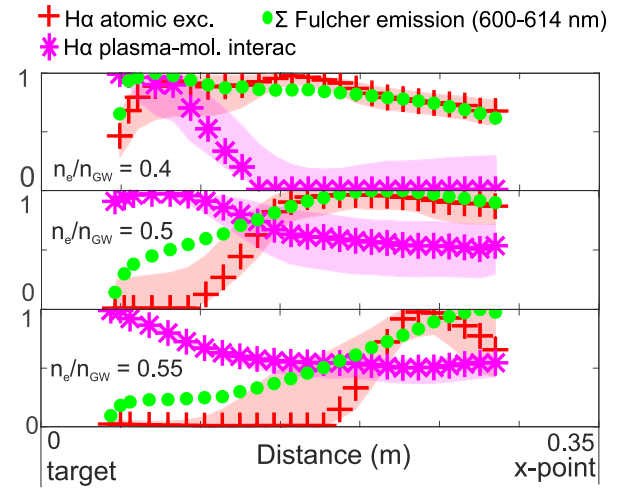


Fig. 4. Spatial profiles at three different times/core Greenwald fractions ( $n_e/n_{GW}$ ) (of the same discharge as shown throughout the paper) of normalised (to the maximum)  $H\alpha$  atomic excitation emission,  $H\alpha$  combined emission due to plasma-molecule interactions ( $H_2^+$ ,  $H^-$ ,  $H_2$ ) and summed Fulcher emission between 600 and 614 nm (which has the brightest Fulcher emission lines) with impurity emission lines removed from the spectra.

A second observation is that the Fulcher emission profile spatially follows the electron impact excitation (of H) emission profile and thus the ionisation profile. In contrast, the Balmer line emission from excited atoms after reactions with  $H_2^+$  (and possibly  $H^-$ ) occurs below the Fulcher emission region and remains peaked near the target throughout the discharge; this suggests that there is a spatial and temperature ordering of the various molecular processes. Those two observations will be further discussed in Section 4.1.

### 3.2. Particle balance with plasma-molecule interactions

The evidence presented in the previous section suggests plasma-molecule interactions impact hydrogenic atomic line emission significantly. This has implications for particle balance in two ways: (1) When the hydrogenic Balmer spectra is attributed to be solely from

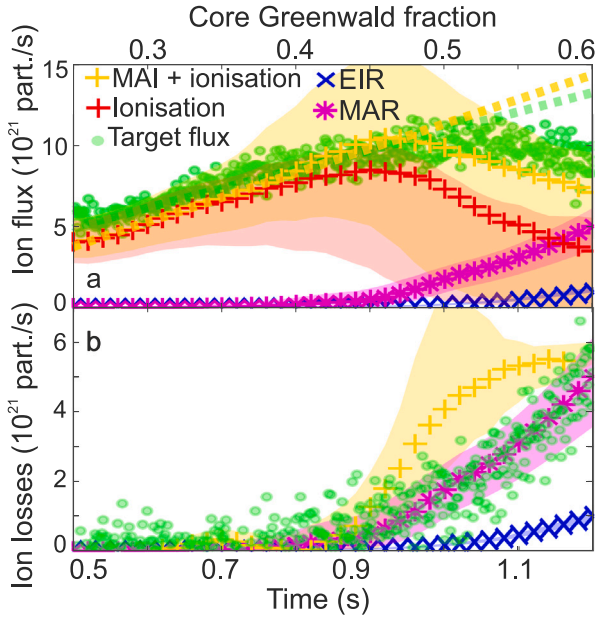


Fig. 5. Inferred particle balance considering plasma–atom and plasma–molecule interactions. This modifies the estimated plasma–atom interaction processes (as it accounts for emission from plasma–molecule interactions in the spectroscopic analysis). (a) Particle balance (ion target current) shown together with estimated atomic ion source, the sum of the atomic and MAI ( $H_2^+$  and  $H_2^-$ ) ion source, EIR sink and total ( $H_2^+$  and  $H_2^-$ ) MAR sink. We have added a linear fit in the attached phase (dotted lines) to the total ion source and ion target flux. (b) Ion losses of the ion target flux, ion sources and through EIR and MAR.

“atomic” interactions (as in [10]), any Balmer line emission from plasma–molecule interactions will be attributed to “atomic processes”; that ‘inflates’ the atomic ion source/sink estimates. (2) When plasma–molecule interactions contribute to, and are properly accounted for, in the Balmer line emission, that indicates the presence of an additional ion sink through Molecular Activated Recombination (MAR) and/or ion source through Molecular Activated Ionisation (MAI).

Particle balance is shown from the perspective of both atomic and plasma–molecule interactions in Fig. 5 for the discharge discussed throughout this paper. The difference in the ionisation estimate between Fig. 5 and Fig. 2 is due to the self-consistent consideration of both plasma–atom ( $H$  and  $H^+$ ) and plasma–molecule interactions (involving  $H_2$ ,  $H_2^+$  and  $H_2^-$ ) leading to excited atoms in Fig. 5. Both the ionisation estimates provide similar results until the detachment onset point ( $n_e/n_{GW} \sim 0.43$ ). After the detachment onset, the estimate of ionisation including plasma–molecule interactions is reduced compared to that obtained when only plasma–atom interactions are included; the EIR ion sink estimate is unaltered.

During detachment, plasma–molecule interactions start to contribute to  $H\gamma$ ,  $H\delta$  (larger impact for lower  $n \rightarrow 2$  compared to higher  $n \rightarrow 2$  transitions) - see Fig. 3. Not including molecular effects leads to an underestimate of the ‘atomic’  $H\delta/H\gamma$  ratio (e.g. higher- $n$ /lower- $n$  ratio), which makes Balmer line emission ‘appear’ to be more excitation rather than recombination dominated [35], leading to a potentially significant ionisation overestimate. We conclude that a self-consistent consideration of plasma–atom and plasma–molecule interactions can be important for inferring information on electron impact excitation (of  $H$ ) emission (and thus ionisation and radiated power from atomic excitation).

The analysis shown in Fig. 5 indicates that MAR is significant at the detached roll-over phase. The onset of MAR occurs between the onset of power limitation (detachment onset) and the onset of EIR ion sinks. The inferred magnitude of MAR for this discharge is  $\sim 5$  times higher

than the magnitude of EIR despite the emission of  $H\gamma$ ,  $H\delta$  (Fig. 3) being EIR dominated.

In this particular case, the MAR ion sink (magenta symbols in Fig. 5a) represents a significant fraction of the ion target flux (green symbols in Fig. 5a) ( $51 \pm 15\%$ ) and thus plays an important role in divertor particle balance.

Plasma–molecule interactions can also increase the ion target flux through MAI. The MAI rate calculated for this case is significant and starts to occur around the detachment onset. The MAI ion source in the detached phase is smaller than the MAR ion sink. These MAI estimates have larger uncertainties and are more sensitive to chordal integration effects as the MAI/ $H\alpha$  photon ratio depends on the relative strength between molecular charge exchange and  $H_2$  ionisation, which is strongly temperature dependent [1]. However, the MAI outcomes are anti-correlated with the atomic ionisation and thus the sum (which has lower uncertainties) of MAI and atomic ion sources is shown in Fig. 5.

Most MAI in this case arises from  $H_2^+$  ions (formed from  $H_2$  ionisation -  $e^- + H_2 \rightarrow 2e^- + H_2^+$ ) in a fairly high temperature regime ( $T_e = [4 - 9]$  eV as opposed to  $T_e = [1.5 - 4]$  eV for MAR) near the electron-impact excitation and Fulcher emission regions, which will be discussed in Section 4.1.

To obtain a more quantitative comparison of the magnitude of ion losses through ion sinks, the reduction of the ion source and the reduction of the target ion flux, the ‘ion losses’ for these different processes are estimated, analogously to [10], and are shown in Fig. 5b. We observe that ion source losses start to occur around the detachment onset and increase from that point onwards. The detachment process starts with the total ion source losses (e.g. including MAI), which seems to be the strongest (together with MAR) contributor to the ion target flux drop. This is followed by MAR and ultimately EIR ion sinks. The magnitude of ion loss due to MAR and the observed ion loss at the target are similar.

The sum of the ion source and sink losses, however, exceeds the estimated ion target flux loss (Fig. 5) during detachment. This suggests the presence of an upstream ion flow towards the target ( $I_u$  - Eq. (3)) during detachment and thus a loss of ‘high recycling conditions’. This contrasts previous findings [10] where only atomic reactions were considered and could arise from ionisation occurring above the spectrometer’s divertor chordal view range (Fig. 2d), which would be consistent with SOLPS-ITER simulations for TCV [38–40].

## 4. Discussion

### 4.1. The evolution of plasma–molecule collisions and reactions during detachment

In Fig. 1 we made the distinction between *collisions* of the plasma and  $H_2$ , exciting  $H_2$  rovibronically and *reactions* between the plasma and  $H_2^+$  (and possibly  $H^-$ ) leading to excited atoms and Balmer line emission. The results from Section 3.1 indicated that the Balmer line emission due to plasma–molecule interactions and Fulcher band emission emit at different locations and evolve differently during detachment. This suggests that there is a large volume in TCV of significant  $H_2$  density extending over a range in  $T_e$ . Different kinds of plasma–molecule interactions dominate at different positions in this volume.

Fulcher band emission occurs when electrons have sufficient energy to electronically excite  $H_2$  ( $T_e > 4$  eV), which likely coincides with the region where  $H_2$  is both dissociated as well as ionised [19]. Therefore, Fulcher band emission should be fairly well localised around the hot part of the separatrix. It is thus surprising that Fulcher band emission occurs throughout the ionisation region given that the  $H_2$  primary source is at/near the target and mean free paths at the target in *attached conditions* are a few centimetres according to simulations [38]. This suggests that molecules enter the divertor leg radially throughout the

ionisation region, which could be attributed to the open, unbaffled divertor structure at the time. According to our analysis, those molecules penetrating into the ionisation region are responsible for the significant levels of MAI inferred (Fig. 5). The measurement that Fulcher emission occurs along the entire divertor leg and follows the ionisation region during detachment (Fig. 4) is qualitatively consistent with estimating the Fulcher emission profile by employing synthetic diagnostics on TCV SOLPS simulations from [38].

These findings seem to be in contrast with filtered camera imaging findings in DIII-D which indicate that (1) Fulcher emission is present [19] in a thin layer close to the target; (2) the Fulcher emission region remains close towards the target during detachment. TCV has longer mean free paths for neutrals (5–10 cm) and molecules than DIII-D which could contribute to this discrepancy (due to lower electron densities, lower heating powers as well as an open divertor). We measure the ionisation front ( $T_e = [4 - 6]$  eV) is lifted  $\sim 20$  cm off the target during our experiment ( $n_e/n_{GW} \sim 0.55$ ). Longer mean free paths and a larger distance between the target and ionisation front would facilitate a larger region in which plasma–molecule interactions occur. Additionally, the presence of other carbon emission lines [19] in the bandpass filter during the measurement on DIII-D could also contribute to the Fulcher emission region not detaching from the target.

In comparison to the primary location of Fulcher band emission, most Balmer line emission from  $H_2^+$  (and possibly  $H^-$ ) and thus the MAR ion sink as well as the  $H_2^+$  (and possibly  $H^-$ ) density, remains peaked near the target and extends up until the ionisation region. Near the target during detachment ( $T_e = [1 - 3]$  eV) the electrons have insufficient energy to promote  $H_2$  ionisation. However, *vibrationally excited molecules* still promote the formation of  $H_2^+$  through molecular charge exchange. In other words, at the location where MAR occurs and most Balmer line emission due to  $H_2$  chemistry is observed, *vibrationally excited molecules* are likely responsible for the formation of  $H_2^+$  (and possibly  $H^-$ ), whereas at the Fulcher band emission region  $H_2$  is *electronically excited*, dissociated and ionised into  $H_2^+$  resulting in MAI.

If there is no longer sufficient energy ( $T_e < [4 - 5]$  eV) for the impact electrons to electronically excite  $H_2$ , this would result in strongly reduced Fulcher band emission. Our results indeed indicate that the Fulcher band emission is particularly dim below the ionisation region where most molecules (as well as MAR) are expected to be present. This may have implications for the applicability of using *only* Fulcher band analysis to diagnose MAR.

Although the mean-free-paths *between the target and the ionisation region* for  $H_2$  are fairly large in detached conditions due to the lower electron temperatures, the expected mean free paths of  $H_2^+$  and  $H^-$ , are much smaller. Potentially, transport of vibrationally excited molecules between the target and the ionisation front (and their interaction with the wall [16]) may play a role in achieving the higher vibrationally excited states near the target. Additionally, if electron impact collisions with  $H_2$  have no longer enough energy to *electronically excite*  $H_2$  ( $T_e < [4 - 5]$  eV) a larger proportion of the energy transfer during those collisions could go into raising the *vibrational levels* in the electronic ground state, which is consistent with measurements and (vibrational-state resolved) simulations [17].

#### 4.2. Evolution of hydrogenic line emission with plasma–molecule interactions and opacity

Our TCV results also indicate a spatial separation due to plasma–molecule interactions during detachment between the measured  $H\alpha$  ( $/Ly\beta - n = 3$ ) and inferred (by extrapolating the individual emission processes)  $Ly\alpha$  emission regions as shown in Fig. 6.

Fig. 7 shows a TCV SOLPS simulation from [38], which is first post-processed to obtain Balmer line emissivities which include plasma–molecule interactions (Section 2) and further post-processed using ray-tracing to estimate where the emission gets absorbed due to opacity. This shows  $Ly\alpha$  and  $Ly\beta$  opacity is negligible on TCV ( $< 5\%$ ), hence

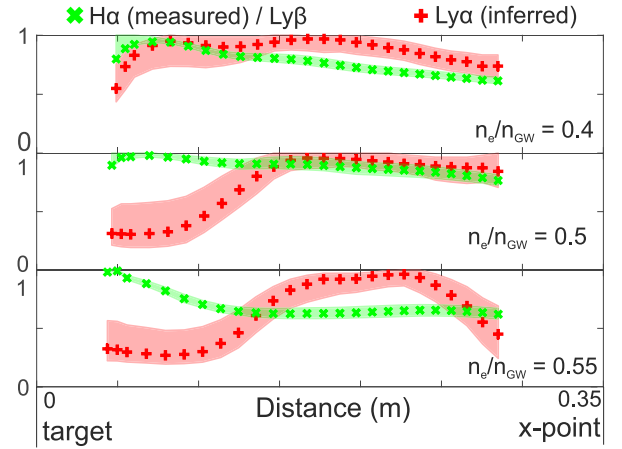


Fig. 6. Normalised profiles (along the different spectroscopic chords) of the measured  $H\alpha$  (and thus  $Ly\beta$ ) emission and the inferred  $Ly\alpha$  emission at three different core Greenwald fractions.

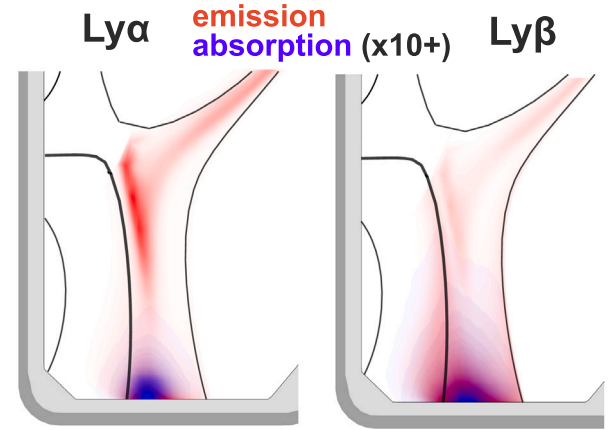


Fig. 7. Schematic overview of  $Ly\alpha$  and  $Ly\beta$  absorption/emission based on ray-tracing obtained from post-processing a SOLPS-ITER simulation (# 106278 [38]) of a detached TCV discharge. As  $Ly\alpha$ ,  $Ly\beta$  opacity is negligible ( $< 5\%$ ), the magnitude of opacity is amplified in the figure for visibility. Emission/absorption from the inner target is omitted as the absorption there is not calculated to reduce computational time.

we amplified the absorption in Fig. 7 for visibility. Plasma–molecule interactions enhance  $H\alpha$  predominantly near the target resulting in a spatial separation of the  $Ly\alpha$  and  $Ly\beta$  emission regions, qualitatively consistent with Fig. 6. As a result,  $Ly\beta$  emits in a region where opacity is (relatively) more dominant than for  $Ly\alpha$ , due to the higher neutral densities near the target; significantly enhancing  $Ly\beta$  opacity.

Although photon opacity is expected to be insignificant for the TCV case studied here, opacity could play a stronger role in other devices such as JET, C-Mod and MAST-U where the photons traverse an integrated neutral density higher than  $10^{18} m^{-2}$  [27,41,42]. Post-processing MAST-U SOLPS-ITER simulations from [29] indicates significant opacity levels for  $Ly\alpha$  and  $Ly\beta$ , whose emission regions are also separated resulting in a relatively higher opacity for  $Ly\beta$ . The separation of the  $Ly\alpha$  and  $Ly\beta$  emission regions could have implications for the diagnosis and understanding of (photon) opacity as using  $Ly\beta$  opacity measurements to model the  $Ly\alpha$  opacity (or the influence of opacity on the ionisation and recombination rates) [27,41,42] requires assuming that  $Ly\alpha$  and  $Ly\beta$  emit and are opaque at the same regions along the line of sight. The development of spatially resolved  $Ly\alpha$ ,  $Ly\beta$  (as well as the Balmer series) diagnostics on tokamak divertors may be required.



#### 4.3. Implications for other devices

This work highlights the importance of including plasma–molecule interactions in divertor plasma physics studies. There are several differences which could occur between these TCV results and other devices/conditions:

1. Our research shows plasma–molecule interactions affect particle balance in a specific temperature regime  $1 < T_i < 2.5$  eV - Fig. 2. If the divertor remains detached while  $T_i > 2.5$  eV, plasma–molecule interactions with  $H_2^+$  (and possibly  $H^-$ ) may not play a strong role. Furthermore, the importance of MAR is reduced in  $T_i < 1$  eV detached conditions where 3-body recombination rises strongly and the EIR/MAR ratio is increased.
2. The transport of molecules and vibrational states in the molecular cloud may be different on TCV than other tokamaks due to differences in: (1) divertor geometry (e.g. baffled vs non-baffled, divertor chamber walls tight around the divertor leg); (2) wall material [16] (e.g. carbon vs tungsten); (3) molecular mean free paths (reduced with higher electron densities and heat fluxes). The transport of  $H_2$  to higher temperature regions (Sections 3.1 and 4.1) where MAI occurs may be related to the open TCV geometry and relatively large molecular mean free paths.
3. Higher electron densities than on TCV ( $n_e \sim 10^{20} \text{ m}^{-3}$ ) could increase the EIR/MAR ratio as electron–ion recombination scales with the power 2–3 of the electron density [41,43] while the plasma–molecule processes influencing MAR and MAI increase less quickly with electron density.
4. The formation mechanisms of  $H_2^+$  and  $H^-$  are believed to be highly isotope dependent and could be different in deuterium–tritium plasmas.

Although differences may exist between TCV and conditions on other devices, experimental findings from both DIII-D [19] and JET [27] using deuterium plasmas are also suggestive of plasma–molecule interactions influencing  $H\alpha$ . At DIII-D [19], the measured  $H\alpha/H\beta$  line ratios were more than a factor 5 higher than that expected based on atomic interactions, which is in agreement with our TCV measurements.

Therefore, the importance of plasma–molecule interactions raised in this work may be generally applicable to other tokamaks with both deuterium and protium plasmas and further investigations on other devices are required.

#### 5. Summary

In this work we have applied new spectroscopic analysis techniques developed in [1] to investigate the impact of plasma–molecule interactions on the detachment process in TCV during core density ramp discharges. Multi-step plasma–molecule interaction processes produce  $H_2^+$  (and possibly  $H^-$ ) followed by the breakup of those species which leads to both Molecular Activated Recombination (MAR) as well as Molecular Activated Ionisation (MAI). Those reactions result in excited atoms, leading to enhancements of the Balmer series emission. We find that the impact of these reactions on both particle balance and the Balmer series emission is significant during detachment.

For our studied discharge, MAR results in  $\sim 5$  times more ion loss than electron–ion recombination. While MAR is concentrated in the detached region it occurs at higher temperatures (up to 2.5 eV) than for 3-body recombination ( $< 1$  eV).

Balmer line emission attributed to  $H_2$  chemistry remains peaked at the target while  $H_2$  Fulcher emission ‘detaches’ from the target, following the ionisation region, as detachment proceeds. This suggests that there is a spatial separation between the various plasma–molecule interactions.

The strong enhancement of Balmer line emission near the target attributed to plasma–molecule interactions indicates enhancements in the Lyman series, potentially impacting power losses. These enhancements

are expected to result in a separation of the  $Ly\alpha$  and  $Ly\beta$  emission regions which would likely lead to changes of the effects and location of opacity.

It appears that attributing the enhancements to Balmer series emission during detachment just to plasma–atom interactions can lead to an inaccurate description of divertor particle balance.

#### CRediT authorship contribution statement

**Kevin Verhaegh:** Conceptualization, Methodology, Software, Formal analysis, Investigation, Writing - original draft, Visualization, Funding acquisition. **Bruce Lipschultz:** Conceptualization, Methodology, Resources, Writing - review & editing, Funding acquisition. **James Harrison:** Conceptualization, Writing - review & editing, Funding acquisition. **Basil Duval:** Conceptualization, Methodology, Resources. **Chris Bowman:** Formal Analysis. **Alexandre Fil:** Investigation. **Daljeet Singh Gahle:** Conceptualization. **David Moulton:** Validation. **Omkar Myatra:** Investigation. **Artur Perek:** Conceptualization. **Christian Theiler:** Resources. **Mirko Wensing:** Software, Validation.

#### Declaration of competing interest

The authors declare that they have no known competing financial interests or personal relationships that could have appeared to influence the work reported in this paper.

#### Acknowledgements

This work has received support from EPSRC Grant EP/T012250/1 and has been carried out within the framework of the EUROfusion Consortium and has received funding from the Euratom research and training programme 2014–2018 and 2019–2020 under grant agreement No 633053. This work as supported in part by the Swiss National Science Foundation. The views and opinions expressed herein do not necessarily reflect those of the European Commission.

#### References

- [1] K. Verhaegh, B. Lipschultz, C. Bowman, B.P. Duval, U. Fantz, A. Fil, J.R. Harrison, D. Moulton, O. Myatra, D. Wunderlich, F. Federici, D.S. Gahle, A. Perek, M. Wensing, A novel hydrogenic spectroscopic technique for inferring the role of plasma–molecule interaction on power and particle balance during detached conditions, *Plasma Phys. Control. Fusion* 63 (3) (2021) 035018, <http://dx.doi.org/10.1088/1361-6587/abd4c0>.
- [2] R.A. Pitts, S. Carpentier, F. Escourbiac, T. Hirai, V. Komarov, S. Lisgo, A.S. Kukushkin, A. Loarte, M. Merola, A.S. Naik, R. Mitteau, M. Sugihara, B. Bazylev, P.C. Stangeby, A full tungsten divertor for ITER: Physics issues and design status, *J. Nucl. Mater.* 438 (2013) S48–S56, <http://dx.doi.org/10.1016/j.jnucmat.2013.01.008>.
- [3] A. Loarte, B. Lipschultz, A.S. Kukushkin, G.F. Matthews, P.C. Stangeby, N. Asakura, G.F. Counsell, G. Federici, A. Kallenbach, K. Krieger, A. Mahdavi, V. Philipps, D. Reiter, J. Roth, J. Strachan, D. Whyte, R. Doerner, T. Eich, W. Fundamenski, A. Herrmann, M. Fenstermacher, P. Ghendrih, M. Groth, A. Kirschner, S. Konoshima, B. LaBombard, P. Lang, A.W. Leonard, P. Monier-Garbet, R. Neu, H. Pacher, B. Pegourie, R.A. Pitts, S. Takamura, J. Terry, E. Tsitrone, I.S.-o.L.D. Phy, Chapter 4: Power and particle control, *Nucl. Fusion* 47 (6) (2007) S203–S263, <http://dx.doi.org/10.1088/0029-5515/47/6/S04>.
- [4] J.A. Goetz, C. Kurz, B. LaBombard, B. Lipschultz, A. Niemczewski, G.M. McCracken, J.L. Terry, R.L. Boivin, F. Bombarda, P. Bonoli, C. Fiore, S. Golovato, R. Granetz, M. Greenwald, S. Horne, A. Hubbard, I. Hutchinson, J. Irby, E. Marmar, M. Porkolab, J. Rice, J. Snipes, Y. Takase, R. Watterson, B. Welch, S. Wolfe, C. Christensen, D. Garnier, D. Jablonski, D. Lo, D. Lumma, M. May, A. Mazurenko, R. Nachtrieb, P. OShea, J. Reardon, J. Rost, J. Schachter, J. Sorci, P. Stek, M. Umansky, Y. Wang, Comparison of detached and radiative divertor operation in Alcator C-Mod, *Phys. Plasmas* 3 (5) (1996) 1908–1915, <http://dx.doi.org/10.1063/1.871986>.
- [5] B. LaBombard, J.A. Goetz, I. Hutchinson, D. Jablonski, J. Kesner, C. Kurz, B. Lipschultz, G.M. McCracken, A. Niemczewski, J. Terry, A. Allen, R.L. Boivin, F. Bombarda, P. Bonoli, C. Christensen, C. Fiore, D. Garnier, S. Golovato, R. Granetz, M. Greenwald, S. Horne, A. Hubbard, J. Irby, D. Lo, D. Lumma, E. Marmar, M. May, A. Mazurenko, R. Nachtrieb, H. Ohkawa, P. OShea, M. Porkolab, J. Reardon, J. Rice, J. Rost, J. Schachter, J. Snipes, J. Sorci, P. Stek,



- Y. Takase, Y. Wang, R. Watterson, J. Weaver, B. Welch, S. Wolfe, Experimental investigation of transport phenomena in the scrape-off layer and divertor, *J. Nucl. Mater.* 241 (1997) 149–166, [http://dx.doi.org/10.1016/S0022-3115\(96\)00502-8](http://dx.doi.org/10.1016/S0022-3115(96)00502-8).
- [6] C.S. Pitcher, P.C. Stangeby, Experimental divertor physics, *Plasma Phys. Control. Fusion* 39 (6) (1997) 779–930, <http://dx.doi.org/10.1088/0741-3335/39/6/001>.
- [7] B. Labombard, J. Goetz, C. Kurz, D. Jablonski, B. Lipschultz, G. McCracken, A. Niemczewski, R.L. Boivin, F. Bombarda, C. Christensen, S. Fairfax, C. Fiore, D. Garnier, M. Graf, S. Golovato, R. Granetz, M. Greenwald, S. Horne, A. Hubbard, I. Hutchinson, J. Irby, J. Kesner, T. Luke, E. Marmar, M. May, P. Oshea, M. Porkolab, J. Reardon, J. Rice, J. Schachter, J. Snipes, P. Stek, Y. Takase, J. Terry, G. Tinios, R. Watterson, B. Welch, S. Wolfe, Scaling and transport analysis of divertor conditions on the Alcator C-mod tokamak, *Phys. Plasmas* 2 (6) (1995) 2242–2248, <http://dx.doi.org/10.1063/1.871248>.
- [8] P. Stangeby, The plasma boundary of magnetic fusion devices, in: P. Stangeby (Ed.), *The Plasma Boundary of Magnetic Fusion Devices*, in: *Series in Plasma Physics*, vol. 7, Taylor & Francis, 2000.
- [9] P.C. Stangeby, Basic physical processes and reduced models for plasma detachment, *Plasma Phys. Control. Fusion* 60 (4) (2018) 044022, <http://dx.doi.org/10.1088/1361-6587/aaac6f>.
- [10] K. Verhaegh, B. Lipschultz, B. Duval, O. Février, A. Fil, C. Theiler, M. Wensing, C. Bowman, D. Gahle, J. Harrison, B. Labit, C. Marini, R. Maurizio, H. de Oliveira, H. Reimerdes, U. Sheikh, C. Tsui, N. Vianello, W. Vijvers, An improved understanding of the roles of atomic processes and power balance in divertor target ion current loss during detachment, *Nucl. Fusion* 59 (126038) (2019) <http://dx.doi.org/10.1088/1741-4326/ab4251>.
- [11] B. Lipschultz, J.L. Terry, C. Boswell, J.A. Goetz, A.E. Hubbard, S.I. Krasheninnikov, B. LaBombard, D.A. Pappas, C.S. Pitcher, F. Wising, S. Wukitch, The role of particle sinks and sources in Alcator C-mod detached divertor discharges, *Phys. Plasmas* 6 (5) (1999) 1907–1916, <http://dx.doi.org/10.1063/1.873448>.
- [12] S.I. Krasheninnikov, A.S. Kukushkin, Physics of ultimate detachment of a tokamak divertor plasma, *J. Plasma Phys.* 83 (5) (2017) 155830501, <http://dx.doi.org/10.1017/S0022377817000654>.
- [13] A.A. Pshenov, A.S. Kukushkin, S.I. Krasheninnikov, Energy balance in plasma detachment, *Nucl. Mater. Energy* 12 (2017) 948–952, <http://dx.doi.org/10.1016/j.nme.2017.03.019>.
- [14] P.C. Stangeby, S. Chaofeng, Strong correlation between D 2 density and electron temperature at the target of divertors found in SOLPS analysis, *Nucl. Fusion* 57 (5) (2017) 056007, <http://dx.doi.org/10.1088/1741-4326/aa5e27>.
- [15] B. Lomanowski, M. Carr, A. Field, M. Groth, S. Henderson, J. Harrison, A. Huber, A. Jarvinen, K. Lawson, C. Lowry, A. Meigs, S. Menmuir, M. O'Mullane, M. Reinke, C. Stavrou, S. Wiesen, Spectroscopic investigation of N2 and Ne seeded induced detachment in JET ITER-like wall, *Nucl. Mater. Energy* 20 (100676) (2019), <http://dx.doi.org/10.1016/j.nme.2019.100676>.
- [16] U. Fantz, Emission spectroscopy of hydrogen molecules in technical and divertor plasmas, *Contrib. Plasma Phys.* 42 (6–7) (2002) 675–684, [http://dx.doi.org/10.1002/1521-3986\(200211\)42:6/7<675::Aid-Ctp675>3.0.Co;2-6](http://dx.doi.org/10.1002/1521-3986(200211)42:6/7<675::Aid-Ctp675>3.0.Co;2-6).
- [17] U. Fantz, D. Reiter, B. Heger, D. Coster, Hydrogen molecules in the divertor of ASDEX upgrade, *J. Nucl. Mater.* 290 (2001) 367–373, [http://dx.doi.org/10.1016/S0022-3115\(00\)00638-3](http://dx.doi.org/10.1016/S0022-3115(00)00638-3).
- [18] M. Sakamoto, A. Terakado, K. Nojiri, N. Ezumi, Y. Nakashima, K. Sawada, K. Ichimura, M. Fukumoto, K. Oki, K. Shimizu, N. Ohno, S. Masuzaki, S. Togo, J. Kohagura, M. Yoshikawa, Molecular activated recombination in divertor simulation plasma on GAMMA 10/PDX, *Nucl. Mater. Energy* 12 (2017) 1004–1009, <http://dx.doi.org/10.1016/j.nme.2017.05.001>.
- [19] E.M. Hollmann, S. Brezinsek, N.H. Brooks, M. Groth, A.G. McLean, A.Y. Pigarov, D.L. Rudakov, Spectroscopic measurement of atomic and molecular deuterium fluxes in the DIII-D plasma edge, *Plasma Phys. Control. Fusion* 48 (8) (2006) 1165–1180, <http://dx.doi.org/10.1088/0741-3335/48/8/009>.
- [20] M. Groth, E. Hollmann, A. Jaervinen, A. Leonard, A. McLean, C. Samuël, D. Reiter, S. Allen, P. Boerner, S. Brezinsek, I. Bykov, G. Corrigan, M. Fenstermacher, D. Harting, C. Lasnier, B. Lomanowski, M. Makowski, M. Shafer, H. Wang, J. Watkins, S. Wiesen, R. Wilcox, EDGE2D-EIRENE predictions of molecular emission in DIII-D high-recycling divertor plasmas, *Nucl. Mater. Energy* 19 (2019) 211–217, <http://dx.doi.org/10.1016/j.nme.2019.02.035>.
- [21] A.S. Kukushkin, S.I. Krasheninnikov, A.A. Pshenov, D. Reiter, Role of molecular effects in divertor plasma recombination, *Nucl. Mater. Energy* 12 (2017) 984–988, <http://dx.doi.org/10.1016/j.nme.2016.12.030>.
- [22] M. Wischmeier, R.A. Pitts, A. Alfieri, Y. Andrebe, R. Behn, D. Coster, J. Horacek, P. Nielsen, R. Pasqualotto, D. Reiter, A. Zabolotsky, The influence of molecular dynamics on divertor detachment in TCV, *Contrib. Plasma Phys.* 44 (1–3) (2004) 268–273, <http://dx.doi.org/10.1002/ctpp.200>.
- [23] D. Wunderlich, U. Fantz, Evaluation of state-resolved reaction probabilities and their application in population models for He, H, and H2, *Atoms* 4 (4) (2016) <http://dx.doi.org/10.3390/atoms4040026>.
- [24] D. Wunderlich, M. Giacomini, R. Ritz, U. Fantz, Yacora on the web: Online collisional radiative models for plasmas containing H, H2 or He, *J. Quant. Spectrosc. Radiat. Transfer* 240 (2020) 106695, <http://dx.doi.org/10.1016/j.jqsrt.2019.106695>.
- [25] A. Kukushkin, H. Pacher, The role of “momentum removal” in divertor detachment, *Contrib. Plasma Phys.* 56 (6–8) (2016) 711–716, <http://dx.doi.org/10.1002/ctpp.201610048>.
- [26] E. Krishnakumar, S. Denifl, I. Čadež, S. Markelj, N.J. Mason, Dissociative electron attachment cross sections for H<sub>2</sub> and D<sub>2</sub>, *Phys. Rev. Lett.* 106 (2011) 243201, <http://dx.doi.org/10.1103/PhysRevLett.106.243201>.
- [27] B. Lomanowski, M. Groth, I.H. Coffey, J. Karhunen, C.F. Maggi, A. Meigs, S. Menmuir, M. O'Mullane, Interpretation of Lyman opacity measurements in JET with the ITER-like wall using a particle balance approach, *Plasma Phys. Control. Fusion* (2020) <http://dx.doi.org/10.1088/1361-6587/ab7432>.
- [28] J.S. Park, M. Groth, R. Pitts, J.-G. Bak, S. Thatipamula, J.-W. Juhn, S.-H. Hong, W. Choe, Atomic processes leading to asymmetric divertor detachment in KSTAR L-mode plasmas, *Nucl. Fusion* 58 (12) (2018) 126033, <http://dx.doi.org/10.1088/1741-4326/aae865>.
- [29] O. Myatra, D. Moulton, A. Fil, B. Dudson, B. Lipschultz, Taming the flame: Detachment access and control in MAST-U Super-X, *Plasma Surface Interactions conference*, Princeton, US, 2018, [https://www.fusion-cdt.ac.uk/wp-content/uploads/2018/08/Myatra-Omkar-psi\\_poster.pdf](https://www.fusion-cdt.ac.uk/wp-content/uploads/2018/08/Myatra-Omkar-psi_poster.pdf).
- [30] A. Smolders, M. Wensing, S. Carli, H. De Oliveira, W. Dekeyser, B.P. Duval, O. Février, D. Gahle, L. Martinelli, H. Reimerdes, C. Theiler, K. Verhaegh, the TCV team, Comparison of high density and nitrogen seeded detachment using SOLPS-ITER simulations of the tokamak configuration variable, *Plasma Phys. Control. Fusion* 62 (12) (2020) 125006, <http://dx.doi.org/10.1088/1361-6587/abbcc5>.
- [31] D. Moulton, G. Corrigan, J.R. Harrison, B. Lipschultz, Neutral pathways and heat flux widths in vertical- and horizontal-target EDGE2d-EIRENE simulations of JET, *Nucl. Fusion* 58 (9) (2018) 096029, <http://dx.doi.org/10.1088/1741-4326/aac0f0>.
- [32] M. O'Mullane, ADAS: Generalised collisional radiative data for hydrogen, 2013, <http://www.adas.ac.uk>.
- [33] H.P. Summers, W.J. Dickson, M.G. O'Mullane, N.R. Badnell, A.D. Whiteford, D.H. Brooks, J. Lang, S.D. Loch, D.C. Griffin, Ionization state, excited populations and emission of impurities in dynamic finite density plasmas: I. The generalized collisional-radiative model for light elements, *Plasma Phys. Control. Fusion* 48 (2) (2006) 263–293, <http://dx.doi.org/10.1088/0741-3335/48/2/007>.
- [34] D. Reiter, M. Baelmans, P. Börner, The EIRENE and B2-EIRENE codes, *Fusion Sci. Technol.* 47 (2) (2005) 172–186, <http://dx.doi.org/10.13182/FST47-172>.
- [35] K. Verhaegh, B. Lipschultz, B. Duval, A. Fil, M. Wensing, C. Bowman, D. Gahle, Novel inferences of ionisation & recombination for particle/power balance during detached discharges using deuterium Balmer line spectroscopy, *Plasma Phys. Control. Fusion* 61 (125018) (2019) <http://dx.doi.org/10.1088/1361-6587/ab4f1e>.
- [36] D. Reiter, et al., The EIRENE Code User Manual, Forschungszentrum Jülich GmbH, 2008, <http://www.eirene.de/manuals/eirene.pdf>.
- [37] S.I. Krasheninnikov, A.Y. Pigarov, D.A. Knoll, B. LaBombard, B. Lipschultz, D.J. Sigmar, T.K. Soboleva, J.L. Terry, F. Wising, Plasma recombination and molecular effects in tokamak divertors and divertor simulators, *Phys. Plasmas* 4 (5) (1997) 1638–1646, <http://dx.doi.org/10.1063/1.872268>.
- [38] A.M.D. Fil, B.D. Dudson, B. Lipschultz, D. Moulton, K.H.A. Verhaegh, O. Février, M. Wensing, Identification of the primary processes that lead to the drop in divertor target ion current at detachment in TCV, *Contrib. Plasma Phys.* 58 (6–8) (2017) <http://dx.doi.org/10.1002/ctpp.201700171>.
- [39] A. Fil, B. Lipschultz, D. Moulton, B.D. Dudson, O. Février, O. Myatra, C. Theiler, K. Verhaegh, M. Wensing, Separating the roles of magnetic topology and neutral trapping in modifying the detachment threshold for TCV, *Plasma Phys. Control. Fusion* 62 (3) (2020) 035008, <http://dx.doi.org/10.1088/1361-6587/ab69bb>.
- [40] M. Wensing, B. Duval, O. Février, A. Fil, D. Galassi, E. Havlickova, A. Perek, H. Reimerdes, C. Theiler, K. Verhaegh, M. Wischmeier, SOLPS-ITER Simulations of the TCV divertor upgrade, *Plasma Phys. Control. Fusion* 61 (085029) (2019) <http://dx.doi.org/10.1088/1361-6587/ab2b1f>.
- [41] J.L. Terry, B. Lipschultz, A.Y. Pigarov, S.I. Krasheninnikov, B. LaBombard, D. Lumma, H. Ohkawa, D. Pappas, M. Umansky, Volume recombination and opacity in Alcator C-Mod divertor plasmas, *Phys. Plasmas* 5 (5) (1998) 1759–1766, <http://dx.doi.org/10.1063/1.872845>.
- [42] K. Behringer, U. Fantz, The influence of opacity on hydrogen excited-state population and applications to low-temperature plasmas, *New J. Phys.* 2 (2000) <http://dx.doi.org/10.1088/1367-2630/2/1/323>, 23–23.
- [43] K. Verhaegh, B. Lipschultz, B.P. Duval, R. Harrison, H. Reimerdes, C. Theiler, B. Labit, R. Maurizio, C. Marini, F. Nespoli, U. Sheikh, C.K. Tsui, N. Vianello, W.A.J. Vijvers, Team, Spectroscopic investigations of divertor detachment in TCV, *Nucl. Mater. Energy* 12 (2017) 1112–1117, <http://dx.doi.org/10.1016/j.nme.2017.01.004>.